Large-scale magnetic fields in GRB outflows: acceleration, collimation, and neutron decoupling

Nektarios Vlahakis* and Arieh Königl†

*Section of Astrophysics, Astronomy & Mechanics, Dept. of Physics, University of Athens, Greece
†Dept. of Astronomy & Astrophysics and Enrico Fermi Institute, University of Chicago

Abstract. Using ideal magnetohydrodynamics we examine an outflow from a disk surrounding a stellar-mass compact object. We demonstrate that the magnetic acceleration is efficient ($\gtrsim 50\%$ of the magnetic energy can be transformed into kinetic energy of $\gamma > 10^2$ baryons) and also that the jet becomes collimated to very small opening angles. Observational implications, focusing on the case of an initially neutron-rich outflow, are discussed in Königl's contribution.

1. IDEAL MAGNETOHYDRODYNAMICS

There is growing evidence in favor of magnetic driving in outflows associated with gamma-ray burst (GRB) sources [e.g., 5, hereafter VK03a; see also Königl's contribution in these Proceedings]. The dynamics of these outflows may be described to zeroth order by the ideal, axisymmetric, hydromagnetic equations, consisting of the Maxwell and momentum equations together with the conservations of baryonic mass and specific entropy. VK03a demonstrated that, under the assumptions of a quasi-steady poloidal magnetic field and of a highly relativistic poloidal velocity, these equations become effectively time-independent and the motion can be described as a frozen pulse, generalizing the so-called "frozen pulse" approximation already known in purely hydrodynamic models of GRB outflows [3]. Introducing the magnetic flux function A, the arclength along a poloidal streamline ℓ, and the operator ∇_s that acts while keeping $s \equiv ct - \ell$ constant, the momentum equation can be written as (see VK03a for details)

$$\gamma\rho_0 \left(\mathbf{V}\cdot\nabla_s\right)\left(\xi\gamma\mathbf{V}\right) = \frac{\left(\nabla_s\cdot\mathbf{E}\right)\mathbf{E} + \left(\nabla_s\times\mathbf{B}\right)\times\mathbf{B}}{4\pi} - \nabla P\,. \tag{1}$$

The large-scale electromagnetic field (**E**, **B**), the bulk flow speed (**V**), and the total ($e^{\pm}$+ radiation) pressure can be written as functions of A and the rest baryon density ρ_0[1]

$$\mathbf{B} = \frac{\nabla_s A\times\hat{\phi}}{\varpi} + \mathbf{B}_\phi\,, \quad \mathbf{E} = -\frac{\Omega}{c}\nabla_s A\,, \quad \mathbf{V} = \frac{A\Omega^2}{4\pi\gamma\rho_0 c^3\sigma_{\rm M}}\mathbf{B} + \varpi\Omega\hat{\phi}\,, \quad P = Q\rho_0^{4/3}\,. \tag{2}$$

Faraday's law and the conservations of specific entropy and mass imply that the functions Ω, Q, and $\sigma_{\rm M}$ are constants of motion, i.e., functions of A. By integrating equation

[1] (z,ϖ,ϕ), and (r,θ,ϕ) denote cylindrical and spherical coordinates, whereas subscripts p and ϕ denote poloidal and azimuthal components, respectively.

(1) along $\mathbf{V}_p$ and $\hat{\phi}$ one gets two additional constants of motion,

$$\mu c^2 = \xi \gamma c^2 - \frac{c^3 \sigma_{\rm M}}{A\Omega} \varpi B_\phi \,, \quad \frac{\mu c^2 x_{\rm A}^2}{\Omega} = \xi \gamma \varpi V_\phi - \frac{c^3 \sigma_{\rm M}}{A\Omega^2} \varpi B_\phi \,, \tag{3}$$

describing the conservation of the ratio (total energy flux)/(mass flux) and of the total specific angular momentum, respectively. The remaining unknowns are the functions $A(r\,,\theta)$ and $\rho_0(r\,,\theta)$. The latter is the solution of Bernoulli's equation [which is obtained after substituting all quantities in the identity $\gamma^2 = 1 + \gamma^2 V_p^2/c^2 + \gamma^2 V_\phi^2/c^2$ using eqs. (2) and (3)], whereas the former controls the shape of the poloidal streamlines and is the solution of the highly nonlinear transfield component of the momentum equation (1).

VK03a integrated the last two equations under the r self-similarity assumption $A = r^F f(\theta)$, which makes it possible (with $\Omega \propto A^{-1/F}$, $Q \propto A^{(4-2F)/3F}$, and constant F, $\sigma_{\rm M}$, μ, and $x_{\rm A}$) to separate the (r, θ) coordinates. The resulting simplified set of ordinary differential equations can be easily integrated. Two types of boundary conditions at the base of the flow were considered: (1) The case of a strong poloidal magnetic field ($B_p \gtrsim B_\phi$), which corresponds to a trans-Alfvénic outflow (since the azimuthal field dominates asymptotically and the flow becomes super-fast). (2) The case of a strong azimuthal field ($B_p \ll B_\phi$), which corresponds to a super-Alfvénic flow.

1.1. Trans-Alfvénic flows

A representative solution is shown in Fig. 1. Looking at panel (*a*), which shows the acceleration, one can distinguish three different regimes:
1) $\varpi_1 < \varpi < \varpi_6$ is the fireball phase. The specific enthalpy ξ decreases, resulting in increasing $\gamma \propto \varpi$ ($\xi\gamma \approx$ const, a characteristic of hydrodynamic acceleration), while the specific Poynting flux remains constant (the field is force free). The electromagnetic field only guides the flow, with the bulk of the collimation occurring in this regime.
2) $\varpi_6 < \varpi < \varpi_8$ is the magnetic acceleration regime. The fluid is cold ($\xi \approx 1$), but γ continues to increase (roughly as $\gamma \propto \varpi$) due to the decreasing specific Poynting flux.
3) $\varpi = \varpi_8$ is the asymptotic cylindrical regime. The final Lorentz factor is of the order of the final specific Poynting flux, meaning that $\sim 1/2$ of the total energy (which was mostly electromagnetic initially) is transformed into baryonic kinetic energy ($\gamma_\infty \approx \mu/2$).

The solution presented in Fig. 1 describes one shell, corresponding to a particular value of s. By specifying the s dependence in the initial conditions one can examine a multiple-shell outflow and the time dependence of the pulse. For example, the s dependence of the (total energy)/mass flux ratio $\mu(s)c^2$ translates into different final Lorentz factors for distinct shells: $\gamma_\infty(s) \approx \mu(s)/2$. In contrast with Michel's solution [1], in which the classical fast magnetosonic point is located at infinity and $\gamma_\infty \approx \mu^{1/3}$, here this point is encountered at a finite height and most of the magnetic acceleration occurs further out, leading asymptotically to $\gamma_\infty(s) \approx \mu(s)/2 \gg \mu(s)^{1/3}$. Thus, not only is the magnetic acceleration highly efficient, but the stronger dependence of $\gamma_\infty(s)$ on the initial conditions [through $\mu(s)$] can lead to a larger contrast in γ_∞ between successive shells and hence to a higher efficiency of internal shocks [e.g., 2].

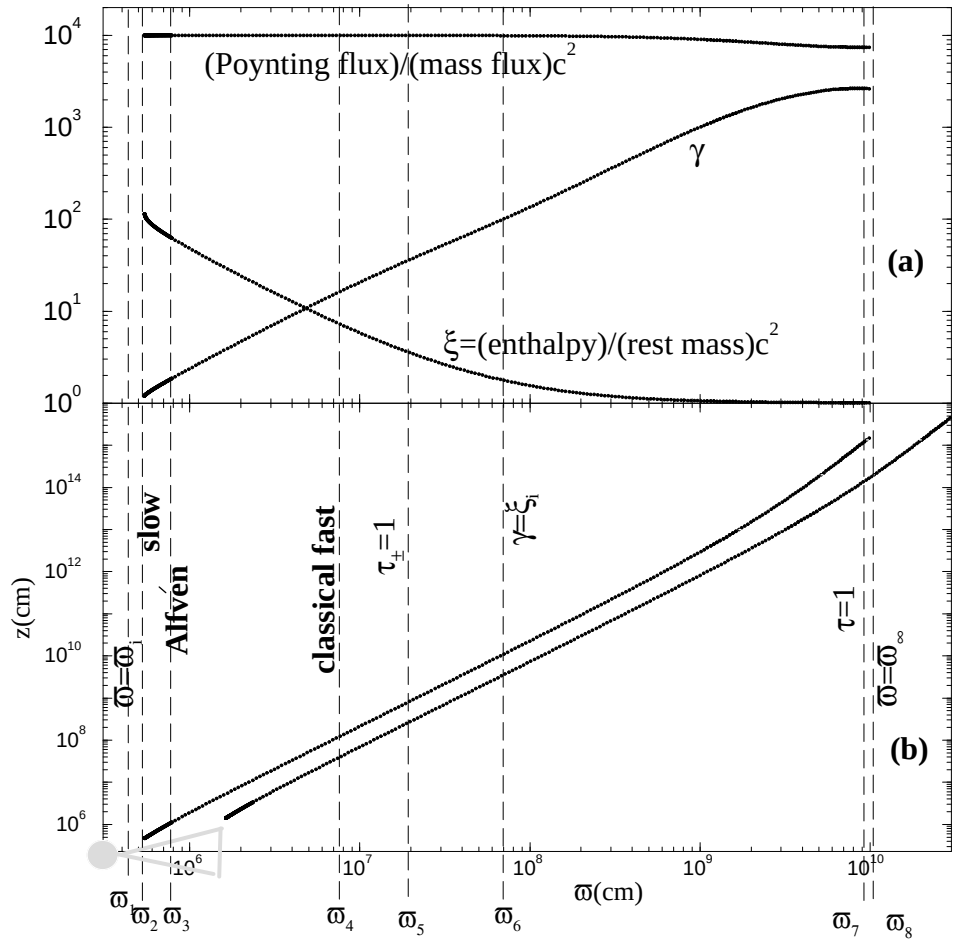

FIGURE 1. Trans-Alfvénic flow solution. (*a*) The Lorentz factor γ, the ratio ξ of the enthalpy to the rest energy, and the ratio of the Poynting flux to the rest-energy flux (*top* curve) are shown as functions of ϖ along the innermost field line. (*b*) The meridional projections of the innermost and outermost field lines are shown on a logarithmic scale, along with a sketch of the central object/disk system. The field lines have a parabolic shape ($z \propto \varpi^2$) for $\varpi \lesssim 10^9$cm and become asymptotically cylindrical. The vertical lines mark the positions of the various transition points along the innermost field line [see text and 4].

1.2. Super-Alfvénic flows

A representative super-Alfvénic solution, corresponding to a base magnetic field ($B_\phi \sim 10^{14}$ G, $B_p \sim 10^{-2}B_\phi$), is shown in Fig. 2. The super-Alfvénic solutions are distinguished from the trans-Alfvénic ones in two main respects: (1) During the initial thermal-acceleration phase, some of the internal energy is transformed into electromagnetic energy even as another part is used to increase V_p. (2) During the subsequent magnetic-acceleration phase, the rate of increase of the Lorentz factor with z can be significantly lower than in the trans-Alfvénic case; the rate of increase of the jet radius with z is correspondingly higher. The overall magnetic-to-kinetic energy conversion efficiency is higher. See [6] for further details and analytic scaling relations.

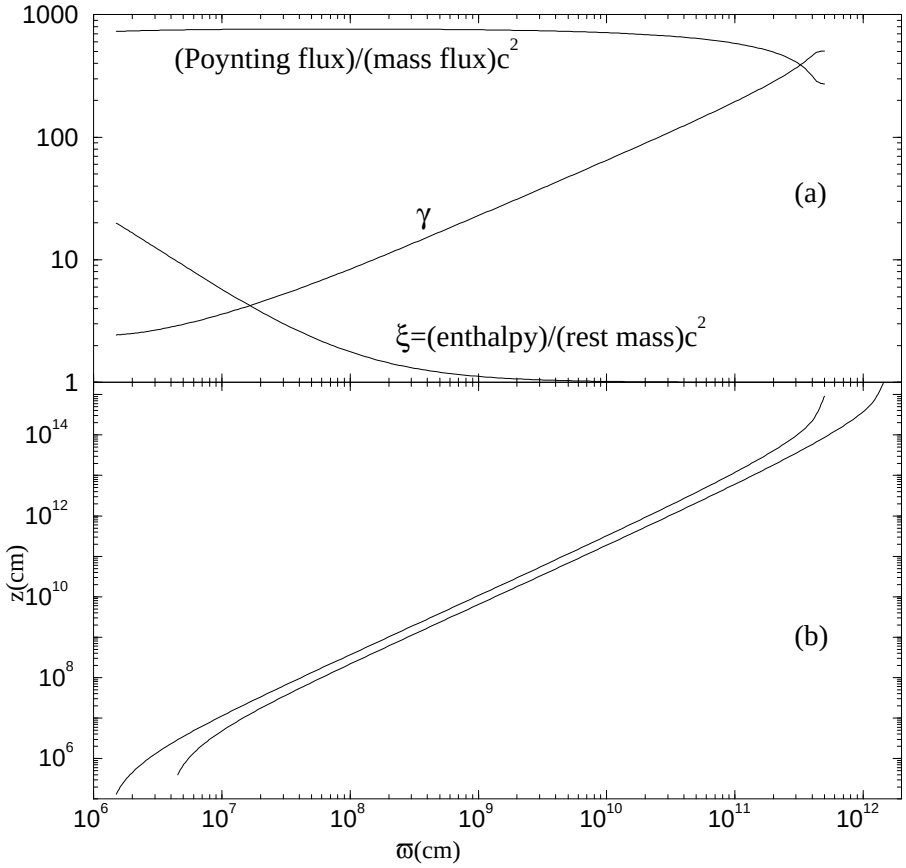

FIGURE 2. Same as Fig. 1, but for a super-Alfvénic solution. Here $\gamma \propto \varpi^{0.46}$, $z \propto \varpi^{1.48}$.

Another potentially important aspect of super-Alfvénic outflows, namely, the possibility that their initial composition is highly neutron-rich, could significantly alleviate the GRB baryon-loading problem. In [7] (see also Königl's contribution) it is shown that, in contrast to the purely hydrodynamic case, the neutrons can decouple at a Lorentz factor that is over an order of magnitude smaller than γ_∞ for the protons.

REFERENCES

1. Michel, F. C. 1969, ApJ, 158, 727
2. Piran, T. 1999, Phys. Rep., 314, 575
3. Piran, T., Shemi, A., & Narayan, R. 1993, MNRAS, 263, 861
4. Vlahakis, N., & Königl, A. 2001, ApJ, 563, L129
5. _____. 2003a, ApJ, 596, 1080 (VK03a)
6. _____. 2003b, ApJ, 596, 1104
7. Vlahakis, N., Peng, F., & Königl, A. 2003, ApJ, 594, L23